Soil-like Deposits Observed by Sojourner, the Pathfinder Rover

Henry J. Moore[1], Donald B. Bickler[2], Joy A. Crisp[2], Howard J. Eisen[2], Jeffrey A. Gensler[3], Albert F. C. Haldemann[2], Jacob R. Matijevic[2], Ferenc Pavlics[4], and Lisa K. Reid[2].

[1] U.S. Geological Survey, Menlo Park, California, [2] Jet Propulsion Laboratory, California Institute of Technology, Pasadena, California, [3] University of Texas, Austin, Texas, [4] Pavlics Engineering, Santa Barbara, California

Abstract Most of the soil-like materials at the Pathfinder landing site behave like moderately dense soils on Earth with friction angles near 34^0-39^0 and are called cloddy deposits. Cloddy deposits appear to be poorly sorted with dust-size to granule-size mineral or rock grains; they may contain pebbles, small rock fragments and clods. Thin deposits of porous, compressible drifts with friction angles near 26^0-28^0 are also present. Drifts are fine grained. Cohesions of both types of deposits are small. There may be indurated soil-like deposits and/or coated or crusted rocks. Cloddy deposits may be fluvial sediments of the Ares-Tiu floods, but other origins, such as ejecta from nearby impact craters, should be considered. Drifts are probably dusts that settled from the Martian atmosphere. Remote-sensing signatures of the deposits inferred from rover observations are consistent with those observed from orbit and Earth.

Introduction

In this paper, we use a number of terms that need to be clarified before proceeding. We use "soil-like" to distinguish the Martian granular deposits from terrestrial soils which are mechanically similar, but contain organic materials. Particles are named according to their diameters, in mm, as follows: cobbles, 256-64; pebbles, 64-4; granules, 4-2; sand, 2-0.062; silt, 0.062-0.005; and clay, 0.005 and less. Dust is composed of clay- and/or silt-size particles. A clod is a fragment or lump of soil-like material or dust and a clodlet a small clod. Cloddy deposits contain clods along with other materials. Correlation of our deposits with "soils" in Table 2 of *Smith et al.*. [1997b] are as follows: (a) drift deposits are "bright soils", (b) surface expressions of

cloddy deposits are "dark soils", (c) disturbed deposits are "disturbed soil", and (d) indurated materials are "pink rock" (or "soil"?). Locations of the soil mechanics experiments are shown in Figure 1. We also refer to the locations of selected features and alpha proton X-ray spectrometer (APXS) sample sites. Maps similar to ours showing these features and sample sites are presented by *Golombek et al.* [this issue] and *McSween et al.* [this issue]. *Golombek et al.* [this issue] also include a table that summarizes rover activities. We also indicate the locations of features and APXS sample sites used in the text by placing the soil mechanics experiment location numbers (Figure 1) in parentheses next to the feature.

Like the Viking landing sites [*Binder et al.*, 1977; *Mutch et al.*, 1977], the Pathfinder site can be described as a surface partly covered by drifts atop soil-like deposits admixed with rocks [*Rover Team*, 1997; *Golombek et al.*, 1997b], but drifts are thin and outcrops are absent. Soil-like deposits and drifts occupy most of the surface because rocks larger than 3 cm only cover about 16.1% of the surface within an annulus 3 m to 6 m around the lander (Sagan Memorial Station); rock coverage is heterogeneous: 10.2% between azimuths 20^0-140^0 east of north and 24.6% between azimuths 165^0-285^0 east of north [*Golombek et al.*, 1997b; *Smith et al.*, 1997b]. There are at least two soil-like deposits at the Station: (1) drift and (2) cloddy. Materials of Mermaid "dune" (12 in Figure 1) may be a third type. A bright-red or "pink" indurated material may be a fourth type [*Rover Team*, 1997; *Smith et al.*, 1997b].

The rover, which was a technology experiment [*Matijevic,* 1998], performed fourteen soil mechanics (Figure 1), six no-load current, and eleven wheel abrasion experiments by the end of Sol 74 and disturbed deposits as it traversed about 105 meters across the surface. Below, we (1) describe the rover and its cameras, the deposits, and the soil mechanics experiment, (2) present results from soil mechanics tests on Earth and results on grain size, friction angle and cohesion for the Pathfinder site, (3) estimate bulk densities, thermal inertias, and radar reflectivities of the soil-like deposits, and (4) discuss our results. Preliminary results have been reported [*Rover Team*, 1997]. Some problems are still unresolved and revisions can be expected at a future date. Mapping of the distributions of some deposits is yet to be performed.

Rover and Cameras

Interactions of the rover with the surface deposits and images taken with the rover cameras [*Rover Team*, 1997, *The Rover Team*, 1997] and the Imager for Mars Pathfinder (IMP or lander camera) [*Smith et al.*, 1997a,b] are essential to understanding the deposits. The rover moves using six wheels powered by separate electric motors and turns using the two forward and two aft wheels which are separately powered by electric motors (Figures 2 and 3). Wheels are linked to the chassis by a rocker-bogie suspension system. The driving surfaces of each of five wheels have thirty-six rows with, alternately, eight and nine cleats or grousers (Figure 2); the center cleats were removed from the right middle wheel for the wheel abrasion experiment [*Ferguson et al.*, this issue]. Wheel motors deliver torques that exceed those required to move the rover up steep slopes. Because the wheels are separately powered, the rover can rotate some wheels with the others locked. This permits the performance of a variety of tasks. Among the tasks are wheel spinning, skidding, plowing, and trenching. Mass, dimensions, and other characteristics of the rover are given in Table 1.

There are three cameras aboard the rover. Two broadband, monochrome cameras are located on the forward part of the rover. A third camera is located on the aft part of the rover near the APXS. The aft camera has three broadband filters which yield some spectral information at the expense of resolution for each color. Characteristics of the rover cameras are given in Table 2 and those of the IMP are given in *Smith et al.* [1997a,b]. Fields of view and lens curvatures are so large that image distortions are severe, especially near the margins. Pre-flight calibrations were performed for the central portions (~ 65^0) of each camera lens so that distortions can and have been removed for the calibrated parts. The forward cameras provide stereoscopic information on surface configurations and calibrated parts of the images permit stereometric measurements of dimensions of small landforms, rocks, and trenches.

Lander [*Smith et al.*, 1997a,b] and rover [*Rover Team*, 1997] camera images were used to: (a) establish the topographic configurations of the surface [*Matijevic,* 1998], (b) locate and identify

targets and experiment sites, (c) position the rover for sampling and other experiments, and (d) assess results and experimental conditions. Rover laser ranging and contact sensors were also used to position the Rover for sampling and other experiments .

Description of Deposits

Bright-red, fine-grained drifts occur as thin, discontinuous ridged sheets and windtails. Drifts are superposed on adjacent deposits and rocks. Rover wheels compress the materials of drifts producing ruts with steep walls, marginal slumps, and reflective molds of the spacings between the cleats (Figure 4; near 9 in Figure 1). In places, pieces of drift are compressed and picked-up by the wheels, transported short distances, and then re-deposited as very bright red coherent flakes a cm across and less (Figure 5; northwest of 2 in Figure 1). Dark indentations and patches are produced where the drift deposits have been plucked from the surface.

In Cabbage Patch (4 in Figure 1), the rover has excavated through an overlying thin layer of drift into poorly-sorted materials which we call cloddy deposits; the cloddy deposits include granule-size clods and/or rock grains (Figure 6). Here, small cm-size rock fragments and pebbles with windtails have probably been exhumed from beneath a superposed drift deposit by natural processes. Evidence for removal of drift deposits at the landing site includes (1) tops of rocks that are darker than their bases [see Fig. 2 in*Smith et al.*, 1997b], (2) sculpted wintails of drifts [*Smith et al.*, 1997b] that are devoid of small rocks, pebbles, and granules, and (3) moats at the bases of rocks with walls of drifts that are devoid of small rocks, pebbles, and granules and floors that are littered with small rocks and other coarse materials. Elsewhere at the site, removal of fine-grained materials from cloddy deposits has resulted in patchy surfaces with residua of small cm-size clods, rock fragments, and well-rounded pebbles [*Rover Team*, 1997]. The patchy surfaces are widespread. Many of these small rock fragments and pebbles that appear to rest on the surface may have been part of an underlying deposit. At least locally, a crust has formed at the surface of cloddy deposits. A different deposit may be indicated for Mermaid "dune" (Figure 7; 12 in Figure 1) because the dark, gray coloration of its northeast-facing surfaces [*Smith et al*, 1997b] and a silica content [*Rieder et al.*, 1997] that is slightly high for most soil-like deposits may be caused by

a veneer or armor of sands and/or granules from rocks too coarse for eolian transport. Exposures, such as Scooby Doo (Figure 8; 5 in Figure 1) [*Smith et al.,* 1997a] , may be indurated soil-like deposits because they form flat-lying surfaces that appear to underlie drift and cloddy deposits, the rover was unable to dig into Scooby Doo, and Scooby Doo has a chemical composition similar to soil-like deposits elsewhere [*Rieder et al.*, 1997]. The rover is unable to excavate strong cohesive deposits like adobe or hardpan on Earth. Preliminary tests with a clayey soil suggest, as a very rough estimate, that the rover could not excavate deposits with cohesions greater than about 3 - 6 kPa. Some "pink" materials, like Scooby Doo, may be coated or crusted rocks [*McSween et al.*, this issue].. About 1 m north of Scooby Doo, equally "pink" Casper (Figure 4; near 9 in Figure 1) resembles a buried coated rock, rather than a soil-like deposit.

Soil Mechanics Experiment

There are three main elements in a standard soil mechanics experiment: (1) rover images, (2) IMP images, and (3) rotations of the rear and front wheels (Table 3, Figure 9; near 2 in Figure 1). Complete sets of information are missing for various reasons, such as insufficient data rates, transmission losses, and sensor failures. Procedures were also altered to fit the circumstances. Often, only one wheel was rotated one-quarter to one and a half revolutions in quarter revolution steps while the remaining five wheels remained locked; rotations were forward for the rear wheels and either backward or forward for the front wheels. Each quarter revolution lasts about 9.5 s and motor currents were sampled about every 0.2 s for 10 ms. Software on Mars discarded the high and low current in each 10 ms interval and averaged the remaining eight values to provide representative values for the currents. Motor currents are reported on Earth with a resolution of 1.48 mA . During experiments on Mars, motor currents rarely exceeded 40 mA, but currents as large as the stall current (Table 1) could be measured. Left and right bogie and rocker differential angles were measured concurrently with the motor currents; resolutions are 0.08^0. These angles are used in conjunction with rover dimensions to estimate wheel depth as a function of time. For

example, the right (or left) bogie axis acts as a pivot for the rocker while the right (or left) rear wheel digs into the surface. Temperatures of the left and right front wheel motors were measured before each quarter turn; rear wheel motor temperatures were not monitored. The temperature sensor for the right front wheel failed early in the mission.

In our analyses, shear or tractive forces are derived from wheel torque and wheel radius [e.g. *Rover Team*, 1997]. According to terrestrial data, torque is a linear function of the motor current above a no-load current and only weakly dependent on temperature. The relations used are:

$$M = y\,(I - x) \tag{1}$$

$$y = 0.4518 - 0.0013 * T \tag{2}$$

where:

M is torque (in inch-lbs),

y is a variable (in inch-pounds / mA),

I is motor current (in mA),

x is a no-load motor current (in mA),

T is the temperature of the wheel motor (in degrees C), and

1 inch-lb = 0.113 N-m.

No-load currents were established on Mars by lifting the two front wheels and right center wheel above the surface, rotating the wheels, and monitoring the motor currents (Figure 10). Nominal no-load currents were obtained for the rear wheels (Table 4) using adjustments indicated for each wheel from tests on Earth because the rear wheels are always on the surface; these tests indicate the right-rear and left-rear wheel no-load currents should be 1 and 2 mA higher than that of the left-front wheel, respectively. The no-load currents from Earth-based tests show a strong temperature dependence, but this is not evident in the no-load currents on Mars. The strong no-load current temperature dependence during the experiments on Earth was probably caused by moisture and icing. For this reason, we have conducted several analyses of the same experiment to

estimate the effects of changes in no-load and the variable "y" above. Further study of this issue is needed.

In our analyses of the properties of the soil-like deposits, we employ the Mohr-Coulomb failure criteria [e.g. *Terzaghi*, 1948]:

$$S = c + N * \tan \Phi, \quad (3)$$

where:

S = shear or tractive stress,

c = cohesion,

N = normal stress, and

tan Φ is the coefficient of friction (Φ is the friction angle).

The apparent friction coefficient, tan α, is:

$$\tan \alpha = S/N = c/N + \tan \Phi. \quad (4)$$

As a first step in our analyses, we estimate the load or normal force on a rear wheel using an heuristic equation that employs shear force, wheel depth, moment arms, and spring constants. In figure 11, we illustrate estimates of the normal forces and apparent friction coefficients (tan α) for the second left rear wheel test of experiment 12. Normal stress is calculated from the estimated normal force, acceleration of gravity, and the projected contact area. Shear stress is calculated from wheel torque, wheel radius, and the projected contact area. The projected area is taken as the product of wheel width and the chord corresponding to the wheel depth (d). Shear (S) and normal (N) stresses are calculated concurrently and have been analyzed in a number of ways [e.g. *Rover Team*, 1997]. Average values of ratios of S and N form our estimate of the apparent friction coefficient (tan α). In cases where the cohesion (c) is small, the apparent friction coefficient (tan

α) is nearly constant. The coefficient of friction (tan Φ) and cohesion (c) are estimated using least squares fits to paired concurrent values of shear and normal stresses (Figure 12). We also fit the paired values to obtain a coefficient of friction (tan Φ_0) and friction angle (Φ_0) assuming that the cohesion is zero. Estimates of slopes or angles of repose (Θ) of piles excavated by the rover were also made by making stereometric measurements on stereoscopic pairs of IMP images [*Rover Team*, 1997] and monoscopic measurements in one case (e.g. Figure 7); slopes of these piles should approximate the friction angles of moderately dense in situ deposits with small cohesions. This approximation is not true for very porous deposits with small cohesions. Our results and experimental conditions are reported in Table 4.

Tests on Earth

Tests were conducted to validate the use of rover wheels to estimate the mechanical properties of soil-like materials using analytical solutions to equations 3 and 4. Three test materials in loose and compacted states (Table 5) were used: (1) well-sorted sand, (2) poorly-sorted sand, and (3) lunar nominal "soil." Grain size distributions for these materials are given in Table 6. Tests were conducted using a flight configuration wheel (which includes the motor) with its drive system connected to a dynamometer to measure tractive or shear force at the wheel radius. The wheel axis was loaded with a weight and rotated to dig into the test material for about 40 secs while tractive force, motor current, and sinkage were monitored. The resulting information was analyzed using the known forces, geometries, calculated stresses, and various forms of the Mohr-Coulomb equation. In separate experiments, wheel loads 4.4, 13.5, and 22.2 N were applied to provide different experimental conditions for each material and state and to cover the expected ranges of normal loads on Mars.

Tests were also conducted using a shear plate (7 cm x 18.9 cm) with cleats identical to those of the flight wheel. The plate was loaded with weights and pulled horizontally while shear forces were measured with a load-cell. The weights or normal loads were 0.57 (the plate), 6.97,

13.6, 24.8, and 35.9 N. Plots of horizontal force and time were analyzed to identify forces corresponding to failure. Friction angle and cohesion were obtained from a plot comparing the shear and normal stresses for each test material.

Friction angles and cohesions from the wheel tests are in reasonable agreement and less than few degrees ($< 3^0$) smaller than those from the shear plate tests. (Table 5). Likewise, cohesions from wheel tests are only less than few tenths of a kPa (< 0.19 kPa) larger than those from the shear plate tests. Our friction angles from shear plate tests are in reasonable agreement with, but somewhat larger than, those from similar tests for Lunar Roving Vehicle studies [*Costes et al.*, 1972] and cohesions are substantially smaller (Table 5). Results for triaxial shear tests from Lunar Roving Vehicle studies [*Costes et al.*, 1972] are also included in Table 5.

Grain size

Two lines of evidence indicate there are significant amounts of fine particles or dust in the soil-like deposits: the wheel abrasion experiment and wheel tracks. Dust can be seen adhering to the rover wheels in early images and enhanced, but variable, dust adhesion is implied by the reduced reflectances of the strips of nickel, platinum, and aluminum (Figures 2 and 3) measured during the wheel abrasion experiment [*Rover Team*, 1997]. This adhesion has been attributed to electrostatic charging which results in the attraction of dusts during traverses on deposits containing grains about 20-40 microns and less [*Rover Team*, 1997; *Ferguson et al.*, this issue]. Commonly, the rover tracks have low to non-existent rims and bright reflective surfaces (Figures 4, 5, 7, and 13); such tracks are produced in soil-like deposits with grains less than about 40 microns, but not in sand [*The Rover Team*, 1997]. The grain size of the lunar regolith was constrained using similar methods during the Surveyor Lunar Program [*Christensen et al.*, 1967]. Rover images of deep excavations in drifts were never obtained because drifts are usually thin and scattered.

Reflective surfaces can be seen in tracks everywhere, but they are less obvious in tracks on the residues of small cm-size clods and fragments associated with cloddy deposits which suggests the presence of sands, granules, clods and/or small rocks, as well as dust (Figures 6 and 9). As noted earlier, the northeast surface of Mermaid (Figure 7, 12 in Figure 1) may have an eolian armor of dust-free sands and/or granules with the same composition as the rocks that are too large to be removed by the wind because the surface is dark for a "soil" [*Smith et al.*, 1997b] and the silica content of the Mermaid surface (sample A15) is larger (by 2%) than most samples of soil-like deposits (A-4, A-5, and A-10) [*Rieder et al.*, 1997]. However, the deposit is not composed entirely of dust-free sands and/or granules because the rover tracks are reflective (Figure 13), excavations in Mermaid show that the deposit is a poorly-sorted mixture (Figure 14), and piles from excavations in Mermaid are red-brown like disturbed soil-like deposits elsewhere (Figure 7). In any event, tracks and excavations suggest most deposits are poorly-sorted mixtures that include dusts, sand- to granule-size clods and/or rock grains, and small pebbles, rock fragments, and clods (Figure 6 and 14).

Friction angle and cohesion

We have re-examined our results on friction angle and cohesion because cohesions were negative for five of sixteen least-squares-fits to concurrent pairs of shear and normal stresses in a previous analysis [*Rover Team*, 1997] and a small modification of our normal force model was indicated. We were able to reduce the occurrence of negative cohesions to two of twenty by excluding the last parts of experiments 3, 8, and 12 where motor currents near the end of the records declined for some unknown reason (excluding experiment 14 and the last part of 13 because the depth-time records indicated the substrate was complicated and hard and, therefore, not amenable to this type of analysis). In the analyses, experiment 11 was unchanged, but the middle part of experiment 10 became negative. The modification of our normal force model had virtually no effect on the results.

Differences between results reported here and previous results are small. The soil-like deposits have mechanical properties (Table 4) that are consistent with moderately dense terrestrial soils, such as a clayey silt that contains some sand, granules, and pebbles [*Hough*, 1957], and a lunar simulant of crushed basalt [*Mitchell et al.*, 1972]. Friction angles average about 34.3^{o} (instead of 36.6^{0}) and are typically between 30^{o} and 40^{o}. The difference in the averages is largely related to the small friction angle obtained in experiment 13. Angles of repose (Θ) measured with lander camera images are between 32.4^{o} and 38.3^{o} (Figures 7 and 9, Table 4). Cohesions average about 0.21 kPa and are typically between 0 and 0.42 kPa. Cohesions are inversely correlated with friction angle ($r^2 = -0.61$, which is statistically significant at the 99% confidence interval for a sample of 20).

We found that changes in results are small when the variable "y" of equation 2 and no-load current are varied. For experiment 11, an increase of "y" from 0.4530 to 0.4712 changed the friction angles less than 0.9^{0} and cohesions less than 0.02 kPa. A reduction in the no-load current from 11.3 to 10.3 mA and "y" from 0.4530 to 0.4712 changed the friction angles less than 0.6^{0} and cohesions by less than 0.02 kPa. These effects will be a subject of future investigations.

Of particular interest is evidence for layering. The depth-time record for experiment 11 (Figure 15A) is inflected and analyses could be divided into two parts (Table 4). For experiment 11, concurrent values of shear and normal stresses yield an upper layer of drift, 1 cm thick, with $\Phi = 27.9^{o}$ and a substrate of the cloddy deposit, more than 3.3 cm thick, with $\Phi = 40.9^{o}$. Thus, evidence for layering during the tests on Mars is consistent with images which show that drift deposits overlie cloddy deposits in the area where the experiment 11 was performed. At Mermaid "dune" (12 in Figure 1), Φ is 34.7^{o} in the upper 1.4 cm and Φ is 37.4^{o} below 1.4 cm where a substrate of cloddy material was excavated. Both layers can be classified as cloddy deposits because the difference in friction angles is small. A rather complicated mix of deposits is indicted in experiment 13 (Figure 15B) because the depth-time record has two peaks near 19 and 24 seconds

and then it flattens. Friction angles suggest a thin 0.3 cm thick layer of drift overlies a cloddy deposit (Table 4). The flat part of the depth-time curve suggests a hard substrate - probably a rock or an indurated material of some sort. Rover images of this experiment were not obtained because data allotments were small and the site is too far from the lander for useful IMP images. Experiment 14 yields results like those of experiment 13. Finally, the depth-time curve for experiment 2 yields no evidence for layering (Figure 15C).

Mechanically, most Ares deposits resemble crusty to cloddy material at the Viking 2 site for which $\Phi = 34.5^{o} \pm 4.7^{o}$ and $c = 1.1 \pm 0.8$ kPa [*Arvidson et al.*, 1989; *Moore and Jakosky*, 1989], but the cohesions at Ares appear to be smaller. For nine values of cloddy deposits at Ares (values with asterisks in table 4), the average $\Phi = 36.7^{o} \pm 3.1^{o}$ and the average $c = 0.18 \pm 0.18$. Scooby Doo (Figure 8, 5 in Figure 1), which wasn't scratched by the rover wheels, may be analogous to the blocky material at the Viking 1 site for which $c = 5.5 \pm 2.7$ kPa and $\Phi = 30.8^{o} \pm 2.4^{o}$, but it could also be a coated rock. The drifts near Casper (Figure 4, near 9 in Figure 1) and elsewhere are very porous and weak because the rover wheels compress them with loads that are only about 1 or 2 kPa. Thus, Pathfinder drifts resemble drift material at the Viking 1 site which is also porous, weak, and fine-grained [*Moore et al.* 1982, 1987] and for which $\Phi = 18.0^{o} \pm 2.4^{o}$ and $c = 1.6 \pm 1.2$ kPa [*Arvidson et al.*, 1989; *Moore and Jakosky*, 1989].

Bulk Density

Bulk density of the soil-like deposits can be crudely estimated from their friction angles assuming they behave like the lunar simulant of *Mitchell et al* . [1972]. From their experiments, Mitchell et al. [1972] found that $\tan\Phi$ was proportional to the reciprocal of the void ratio (e) of the simulant, where void ratio (e) is ratio of volumes of the pores and solids. We estimate that $\tan\Phi = 0.725 * (1/e)$ from their graph. In turn, $e = (\rho s - \rho b) / \rho s$, where ρs and ρb are the grain and bulk

densities, respectively. They give no error bars. We then assume that the densities of the grains are 2,650 and 3,000 kg/m^3. Using 34.3^0 and 36.6^O as a rough estimates of the friction angle, the collective bulk density of the Ares deposits is between 1,285 and 1,518 kg/m^3, respectively. Inferred bulk densities of deposits with the smaller friction angles (26^O-28^O) are near 1,066 -1,269 kg/m^3, while those with the larger friction angles (40^O-41^O) are near 1,422-1,636 kg/m^3. The bulk density of the indurated material is unknown, but it could be rather large, say near 2,000-2,200 kg/m^3, if it is like blocky material at the Viking 1 site [*Moore et al.*, 1987].

Thermal Inertia.

From landed data, the fine-component thermal inertia for the Pathfinder landing site has been estimated at 364 (8.7) (in units of J m^{-2} s$^{-0.5}$ K^{-1} and units of 10^{-3} calories cm^{-2} s$^{-0.5}$ K^{-1} in parenthesis) [*Golombek et al.*, 1997b; *Golombek et al., this issue*]. The estimate is made using the bulk thermal inertia 435 (10.4) from the Viking Infrared Thermal Mapper (IRTM) [Palluconi and Kieffer, 1981], an effective thermal inertia of 1,716 (41) for the entire rock population within the 3 to 6 m annulus [*Golombek et al.*, 1997b], and the mixing model of *Kieffer et al.* [1977]. IRTM rock abundance estimates assume that the entire rock population has a thermal inertia of 1,255 (30) which corresponds to rocks about 10-15 cm across [*Christensen*, 1986a,b]. Our estimate of the effective thermal inertia for the entire rock population is based on the work of Jakosky [1986]. We assume that (a) rocks greater than 0.26 cm have inertias of 2,092 (50) and (b) inertias of rocks < 0.26 cm vary as the 0.75 power of their diameters. Three-cm rocks have inertias near 418 (10). The difference in effective inertias appears to have little effect because our estimated fine-component thermal inertia is in agreement with the fine-component inertia of 352 (8.4) in the IRTM resolution cell that covers the Ares site [*Golombek et al.*, 1997b (from files furnished by P. R. Christensen)]. Similar estimates for the Viking 1 and 2 sites yield fine component inertias of 301 (7.2) and 192-310 (4.6-7.4), respectively (Moore et al., manuscript in preparation, 1998) and compare well with the fine-component inertias of 289 (6.9) and 264 (6.3), respectively, from the IRTM [e.g. *Golombek et al.*, 1997b (from files furnished by P. R. Christensen)]. The effective

thermal inertias for the entire rock populations at the Lander 1 and 2 sites were 1,548 and 1,799 (37 and 43), respectively, and reflect the differences in rock-size frequency distributions at the sites [e.g., *Moore and Keller*, 1990, 1991]. These inertias are smaller than the estimate for Pathfinder 364 (8.7) which is consistent with the large amounts of drifts (assumed inertia of 125 (3)) at the Viking sites where thick (>2 cm) drifts cover 18-30% of the surface and at Lander 1 where thick and thin drifts (> 1 cm) cover 40% of the surface [*Moore and Keller*, 1990] and the sparse amount of drifts at the Pathfinder site.

Viking and Pathfinder observations show that the fine-component thermal inertias are the result of materials more complex than uniform cohesionless particulates [e.g. *Kieffer et al.,* 1973, *Golombek et al.,* 1997a]. Cementation of soil-like materials causes the high fine-component inertias at the Viking sites [Christensen, 1982] because the soil-like deposits are very fine-grained and cohesive [Moore et al., 1987] and appear to be cemented by salts [Clark et al., 1982]; excavations yield no evidence for cohesionless sands. Cemented, poorly-sorted, mixtures of dust, sand, granules, and pebbles cause the high fine-component inertia at the Pathfinder site because cloddy deposits dominate the site and significant amounts of sulfur and chlorine are present in the deposits [*Rieder et al.,* 1997]. Some of the distant dune-forms seen in lander and rover images (Figure 11) could be composed of sand-sized grains with inertias near 259-364 (6.2-8.7) [e.g. *Presley and Christensen*, 1997], but this is unproved because the rover never drove on or excavated into these landforms and then acquired images of the interactions. Later analyses of the IRTM data [*Haberle and Jakosky*, 1991; *Hayashi et al.*, 1995] would yield bulk thermal inertias that are about 106 (2.5) units smaller than those of *Palluconi and Kieffer* [1981]; this would not alter our choices of interpretations.

Radar Reflectivity.

The specular radar echo from a rock-strewn field like the Pathfinder landing site in Ares Vallis is commonly ascribed to the rock-free, flat or gently undulating soil-like surface between the rocks. Thus, the reflectivity parameter in the Hagfors scattering model is then related to the

dielectric constant of the soil-like deposits. In turn, dielectric constants (and reflectivities) are related to the bulk densities of dry silicate powders, soil-like materials, and rocks [*Campbell and Ulrichs,* 1969, *Olhoeft and Strangway,* 1975]. The quasi-specular radar reflectivity of Ares Vallis longitudes in the Chryse region observed before landing is 0.06±0.02 at 3.5-cm wavelength [*Golombek et al.,* 1997a,b, *Haldemann et al.*, 1997]. Larger reflectivities (0.07 to 0.14) are obtained at 12-cm wavelength [*Harmon*, 1997]. These values are averages over very large areas and are therefore entirely consistent with the range of reflectivities displayed by the soil-like deposits examined by Sojourner. Our estimate of the average bulk densities above yields a quasi-specular reflectivity near 0.04 to 0.06 for the surface deposits - excluding the areas covered by rocks [*Olhoeft and Strangway* , 1975; see Figure 5 in *Golombek et al.,* 1997a]; from the equation of *Olhoeft and Strangway* [1975], our calculations yield a 1σ near ± 26% on reflectivity. As viewed by the radar from Earth, this reflectivity would be reduced 84% to 0.034-0.050 because rocks produce diffuse echoes by virtue of their sizes and rough surfaces and reduce the area for quasi-specular reflections [*Evans and Hagfors*, 1964]. Our estimate of the range of reflectivity (0.026-0.064), including 1σ, is in fair agreement with the observed reflectivity at 3.5-cm wavelength. However, the 12 cm reflectivities are greater than those observed at 3.5-cm. Sojourner's observations of layering in deposits suggests that a model with a lower density layer over a more dense layer would be appropriate for the site. Such a model has been proposed for the site [*Harmon*, 1997].

Discussion

Friction angles obtained for the soil-like deposits on Mars using the rover wheels are entirely consistent with terrestrial experience and our tests. We believe the estimates are good ones.

The problem of the magnitudes of the cohesions is still unresolved at this time, but cohesions appear to be generally consistent with terrestrial experience and our tests. The occasional negative cohesions reported earlier [*Rover Team*, 1997] and here are not plausible. We partly

resolved this problem by excluding the latter parts of selected records from our analyses where motor currents declined, but evaluation of the effects of no-load currents, the magnitudes of rate of change of torque with current, and normal force models need to be pursued. We also need to explore the inverse correlation of cohesion with the friction coefficient. Importantly, it should also be realized that the cohesions are small and difficult to estimate (e.g. Figure 12 and Figure 1I in *Rover Team* [1997]).

Cohesions of the Ares deposits may be smaller than those of the deposits at the Viking sites, but differences in the available forces, trench depths, instruments, and analyses procedures make comparisons difficult. In particular, the forces available for Pathfinder were small ($\leq$ 20 N) compared to Viking ($\leq$ 200-225 N), the depths of Pathfinder trenches are small (< 4.5 cm) compared to those of Viking (typically 5-7 cm), Pathfinder analyses used rover wheels instead of a sample scoop, and a wheel model was used to estimate friction angle and cohesion instead of the plowing model used by Viking [*Crouch*, 1977; *McKeyes and Ali*, 1977; *Moore et al.*, 1982, 1987, *Rover Team*, 1997]. These differences will result in biased samples. For example, the rover is unable to excavate strong cohesive deposits like adobe or hardpan on Earth and would not be able to excavate blocky material at the Lander 1 site.

An eolian origin for drifts is likely [*Smith et al.*, 1997b], but the origin of cloddy deposits is unclear. Drifts appear to be composed of dusts that settled from the atmosphere because they are fine-grained, compressible, and the most recent deposits (they are superposed on cloddy deposits, pebbles, small fragments, indurated deposits, and rocks). Cloddy deposits are another matter because they (including Mermaid dune with its dark-gray surface) appear to contain dusts, sand- or granule-size clodlets and/or rock grains, and, perhaps, some pebbles and small rock fragments. Although the presence of sand- and granule-size grains would not preclude an eolian origin, the same origin as the drifts is excluded. Pebbles and small fragments in cloddy deposits would exclude an eolian origin altogether because they are too large for eolian transport. Thus, it is possible that the cloddy deposits are fluvial sediments deposited during some phase of the Ares and Tiu floods.

An impact cratering origin is also possible for the cloddy deposits because ejecta from Big Crater could be tens of centimeters thick [*McGetchin et al.*, 1973]. On the other hand, there could be no ejecta at all because the site is beyond the expectations for limit of continuous ejecta [*Moore, et al.*, 1974].

Origins of the rounded pebbles are an important unresolved problem. They could have been rounded by Ares flood waters and deposited, or rounded by wave or fluvial action elsewhere and transported by the flood waters. Perhaps they have a glacial origin. Could they be drops of solidified impact melts for Big Crater or some distant impact crater? Perhaps they are volcanic fragments or nodules. It is possible that the pebbles were liberated from cloddy deposits or sedimentary rocks by weathering [*Rover Team*, 1997]. The origin of small angular rock fragments is also an unresolved issue.

Pure drifts may never have been chemically analyzed, as indicated by nearby soil mechanics tests, surface morphologies or surface colorations of the APXS sites which are incompatible with drifts. Soil mechanics tests in soil-like deposits near the APXS sites (A-2, 4, 5, 10 and 15) have relatively large apparent coefficients of friction (tan α) or friction angles (Φ) and some have low cohesions (see 1, 2, 3, 4, 8, and 12 in Table 4), but tests in drifts have relatively small values coefficients of friction (tan α) or friction angles (Φ) and large cohesions (see 9 and 11 in Table 4) and are not near any APXS sites. The similar chemical compositions of A-4, A-5, and A-10 suggest that they are the same deposit and the relatively large silica contents of A-15 and A-2 [*Rieder et al.*, 1997] suggest they are different. The first APXS analysis (A-2) may be a mixture of materials because the APXS was deployed onto a complicated surface littered with small rocks and clods and its relatively high silica content [*Rieder et al.*, 1997] suggests that rocks may have been included in the analyses; both the littered appearance of the surface and large value of the coefficients of friction (tan α) for the nearby soil mechanics test (1 in Table 4) suggest cloddy deposits are also present. Sample A-2 also has a small original sum of oxides [*Rieder et al.*, 1997]

which may have been caused by a complicated viewing geometry. The second APXS analysis (A-4) probably represents cloddy deposits because it is adjacent to a soil mechanics experiment (2 in Table 4) that yields an apparent coefficient of friction (tan α) of 0.853 and a friction angle (36.4°) which is consistent with cloddy deposits elsewhere. The surface of the A-5 APXS site appears to have been altered by rover tracks before APXS deployment so that any veneer of drift would have been admixed with subjacent deposits and nearby soil mechanics tests are consistent with cloddy deposits. Results of the soil mechanics experiment adjacent to APXS site A-10 (8 in Table 4) are also consistent with cloddy deposits. Mermaid "dune" (A-15; 12 in Figure 1) is not a drift because of the veneer of dark material and a silica content that is relatively large [*Rieder et al.*, 1997]. Images of Scooby Doo (5 in Figure 1) show that site A-8 is not on a drift. Thus, it is unlikely that "pure" drifts were sampled. Although error bars preclude confident comparisons, the silica contents for analyses of the A-4, A-5, and A-10 deposits are about 3% higher than those the Viking soil-like deposits, when total iron is cast as $Fe_2 O_3$ and the Pathfinder analyses are normalized to 98% total [e.g.*Rieder et al.*, 1997; *Clark et al*, 1982] which suggests that the origin of soil-like deposits at the two sites may be different.

Our results have significance to the surface deposits and remote sensing data elsewhere on Mars. The fine-component thermal inertia and reflectivity inferred for the cloddy deposits, which dominate the site, are entirely consistent with those observed remotely so it appears that judicious interpretations of remote-sensing observations will yield correct answers. The response of drifts to the rover wheels and small friction angles may also be telling us that the regions on Mars where radar reflectivities are small, thermal inertias are low, albedos are high, and red to violet ratios are large, are composed of porous, compressible, dusts.

Conclusions

The dominant materials at Ares are moderately dense soil-like deposits with friction angles typically near 34^0-37^0, but porous, compressible materials with small friction angles are also

present. The former are called cloddy deposits and the latter are called drift deposits. Cohesions of both are small. Cloddy deposits appear to be a mixture of dusts, sand- and granule-size clodlets and/or rock grains, and, possibly, pebbles and small rock fragments. Drifts are fine grained. There may be "pink" indurated soil-like deposits and/or coated rocks.

Cloddy deposits may be products of the Ares-Tiu floods, but other origins should be considered. Drifts are probably dusts that settled from the Martian atmosphere.

Remote-sensing signatures inferred from rover observations are consistent with those observed from orbit and Earth.

Acknowledgments We wish to acknowledge Murray Hirschbein and David Lavery, managers of the NASA the rover development, testing, and operation program, A. Runkle and D. Alexander of MIPL of the Jet Propulsion Laboratory for their tireless support, and S. Arriola of the U.S. Geological Survey for his sustained assistance. None of the Pathfinder rover results would have been possible with out the support of the Rover Operations Team: R.S. Banes, B.K. Cooper, F. Hartman K.A. Jewett, L.H. Matthies, S.L. Laubach, A.H. Mishkin, J.C. Morrison, T.T. Nguyen, A.R. Sirota, H.W. Stone, S. Stride, L.F. Sword, J.A. Tarsala, A.D. Thompson, M.T. Wallace, R. Welch, and B.H. Wilcox. Mike Bennett and Jeff Plescia of the U.S. Geological Survey provided the grain size distributions of test materials. The constructive reviews of Marsha Presley, Jeff Johnson, and Wesley Ward are appreciated. Most of the work described in this paper was carried out by the Jet Propulsion Laboratory, California Institute of Technology, under a contract with the National Aeronautics and Space Administration; H. J. Moore is a Scientist Emeritus of the U.S. Geological Survey.

References

Arvidson, R E, J. L. Gooding, and H. J. Moore, The Martian surface as imaged, sampled, and analyzed by the Viking landers, *Rev. Geophys. Space Phys.*, *27*, 39-60,1989.

Binder, A. B, R E Arvidson, E. A. Guinness, K. L. Jones, E. C. Morris, T. A. Mutch, D. C. Pieri, and C. Sagan, The geology of the Viking Lander 1 site, *J. Geophys. Res.*, *82*, 4439-4451, 1977.

Campbell, M. J. and J. Ulrichs, Electrical properties of rocks and their significance for lunar radar observations, *J. Geophys. Res.*, *74*, 5,867-5,881, 1969.

Christensen, E. M., S. S. Batterson, H. E. Benson, R. Choate, L. D. Jaffe, R. H. Jones, H. Y. Ko, R. L. Spencer, F. B. Sperling, and G. H. Sutton, Lunar surface mechanical properties, in Surveyor III Preliminary Report, *U. S. National Aeronautics and Space Administration Special Publication*, *SP-146*, 94-120, 1967.

Christensen, P. R., Regional dust deposits on Mars: Physical properties, age, and history: *J. Geophys. Res.*, *91*, *B3*, 3,533-3,545, 1986a.

Christensen, P. R., The spatial distribution of rocks on Mars, *Icarus*, *68*, 217-238, 1986b.

Christensen, P. R., Martian dust mantling and surface composition: Interpretation of thermophysical properties: *J. Geophys. Res.*, *87, B12*, 9,985-9,998, 1982.

Clark, B. C., Baird, A. K., Weldon, R. J., Tsusaki, D. M., Schnabel, Lorraine, and Candelaria, M. P., Chemical composition of martian fine, *J. Geophys. Res.*, *87*, *B12*, 10,059-10,067, 1982.

Costes, N. C., Farmer, J. C., and George, E. B., Mobility performance of the Lunar Roving Vehicle: Terrestrial studies - Apollo 15 results, *NASA Technical Report*, *NASA TR R-401*, 78p., 1972.

Crouch, D.S., Mars Viking surface sampler subsystem, in *Proceedings of the 25th Conference on Remote Systems Technology, The American Nuclear Society Anniversary issue*, 141-152, 1977.

Evans, J. V., and T. Hagfors, On the interpretation of radar reflections from the Moon, *Icarus*, *3*, 151-160, 1964.

Ferguson, D. C., Kolecki, M. W. Siebert,, D. M. Wilt, and J. R. Matijevic, Evidence for Martian electrostatic charging and abrasive wheel wear from the wheel abrasion experiment on the Pathfinder Sojourner rover, *this issue*.

Golombek, M.P,, R. A. Cook, H. J. Moore, and T. J. Parker, Selection of the Mars Pathfinder landing site, *J. Geophys. Res.*, *102*, *E2*, 3967-3988, 1997a.

Golombek, M.P,, R. A. Cook, T. Economou, W. M. Folkner, A. F. C. Haldemann, P. H. Kallemeyn, J. M. Knudsen, R. M. Manning, H. J. Moore, T. J. Parker, R. Rieder, J. T. Schofield, P. H. Smith, and R. M. Vaughan, Overview of the Mars Pathfinder Mission and assessment of landing site predictions, *Science*, *278*, 1743-1748, 1997b.

Golombek, M. P., R. C. Anderson, J. R. Barnes, J. F. Bell III, N. T. Bridges, D. T. Britt, J. Brückner, R. A. Cook, D. Crisp, J. Crisp, T. Economou, W. M. Folkner, R. Greeley, R. M. Haberle, R. B. Hargraves, J. A. Harris, A. F. C. Haldemann, K. E. Herkenhoff, S. F. Hviid, R. Jaumann, J. R. Johnson, P. H. Kallemeyn, H. U. Keller1, R. L. Kirk, J. M. Knudsen, S. Larsen, M. Lemmon, M. B. Madsen, J. A. Magalhães, J. N. Maki, M.C. Malin, R. M. Manning, J. Matijevic, H. Y. McSween Jr., H. J. Moore, S. L. Murchie, J. R. Murphy, T. J. Parker, R. Rieder, T. P. Rivellini, J. T. Schofield, A. Seiff, R. Singer, P. H. Smith, L. A. Soderblom, D.A. Spencer, C. Stoker, R. Sullivan, N. Thomas, S. W. Thurman, M. G. Tomasko, R. M. Vaughan, H. Wänke, W. Ward, and G. Wilson, Overview of the Mars Pathfinder Mission: Launch through landing, surface operations, data sets, and science results, *J. Geophys. Res.*, this issue.

Haberle, R. M. and B. M. Jakosky, Atmospheric effects on the remote determination of thermal inertias on Mars, *Icarus*, *90*, 187-204, 1991.

Haldemann, A. F. C., D. L. Mitchell, R. F. Jurgens, M. A. Slade, and D. O. Muhleman, Mars Pahfinder landing site assessment with Goldstone delay-Doppler and CW radar experiments, *J. Geophys. Res., 102*, *E2*, 4097-4106, 1997.

Harmon, J. K., A radar study of the Chryse region, Mars, *J. Geophys. Res.*, *102*, *E2*, 4081-4095, 1997.

Hayashi, J. N. , B. M. Jakosky and R, M. Haberle, Atmospheric effects on the mapping of Martian thermal inertia and thermally derived albedo, *J. Geophys. Res.*, *100*, 5277-5284, 1995

Hough, B. K., *Basic Soils Engineering*, 513pp, Ronald Press Company, New York, 1957.

Jakosky, B. M., On the thermal properties of Martian fines, *Icarus*, *66*, 117-124, 1986.

Kanefsky, B., T.J. Parker, and P.C. Cheeseman, Super-resolution results from Pathfinder IMP, 29th Lunar Planet. Sci. Conf., 1536, 1998.

Kieffer, H. H., S. C. Chase Jr., E. Miner, G. Munch and G. Neugebauer, Preliminary report on infrared radiometric measurements from the Mariner 9 spacecraft, *J. Geophys, Res.*, *78*, 4,291-4,312, 1973.

Kieffer, H. H., T. Z.Martin, A. K. Peterfreund, B. M. Jakosky, E. D.Miner,., and F. D. Palluconi, Thermal and albedo mapping of Mars during the Viking Primary Mission, *J. Geophys. Res.*, *82*, 4,249-4,291, 1977.

Matijevic, J., The Pathfinder Mission to Mars: Autonomous navigation and the Sojourner microrover, *Science*, *280*, 454-455, 1998.

McGetchin, T.R., M. Settle, and J. W. Head, Radial Thickness variation in impact crater ejecta: Implications for lunar basin deposits, *Earth Planet. Sci. Letts*, *20*, 226-236, 1973.

McKyes, E. and O.S. Ali, The cutting of soil by narrow blades, *J. Terramechanics*, *14*, 43-58, 1977.

Mc Sween, H. Y., S. L. Murchie,, J. A. Crisp, N. T. Bridges, Anderson, R. C., J. F. Bell III, D. T. Britt, J. Brückner, G. Dreibus, T. Economou, A.Ghosh, M. P. Golombek, J. P. Greenwood, J. R. Johnson, H. J. Moore, R. V. Morris, T. J. Parker, R. Reider, R. Singer, and H. Wänke, Chemical, multispectral, and textural constraints on the composition and origin of rocks at the Mars Pathfinder landing site, *J. Geophys. Res.*, this issue.

Mitchell, J. K., W. N. Houston, R. F. Scott, N. C. Costes, W. D. Carrier III, and L. G. Bromwell, Mechanical properties of lunar soils: Density, porosity, cohesion, and angle of internal friction, Proceedings Third Lunar Science Conf., Suppl. 3, *Geochim. et Cosmochim. Acta*, *3*, 3235-3253, 1972.

Moore, H. J., C. A. Hodges, and D. H.Scott, Multiringed basins - Illustrated by Orientale and associated features, Proceeding Fifth Lunar Science Conf., Suppl. 5, *Geochim et Cosmochim Acta*, *1*, 71-100, 1974.

Moore, H. J. and B. M. Jakosky, Viking landing sites, remote sensing observations, and physical properties of Martian surface materials, *Icarus*, *81*, 164-184, 1989.

Moore, H. J. and J. M. Keller, Surface material maps of the Viking landing sites on Mars (abstract), in *Reports of Planetary Geology and Geophysics Program - 1989, National Aeronautics and Space Administration Technical Memorandum 4210*, 533-535, 1990.

Moore, H. J. and J. M. Keller, Surface material maps of the Viking landing sites on Mars (abstract), in *Reports of Planetary Geology and Geophysics Program - 1990, National Aeronautics and Space Administration Technical Memorandum 4300*, 160-162, 1991.

Moore, H. J., G. D. Clow, and R. E. Hutton, A summary of Viking sample trench analyses for angles of internal friction and cohesion, *J. Geophys. Res.*, *87*, 10,043-10,050, 1982.

Moore, H. J., G. D. Clow, R. E. Hutton, and C. R. Spitzer, Physical properties of the surface materials at the Viking landing sites on Mars, *U.S. Geol. Survey Prof. Paper 1389*, 222pp., 1987.

Mutch, T. A., R. E. Arvidson, A. B. Binder, E. A. Guinness, and E. C. Morris, The geology of the Viking Lander 2 site, *J. Geophys. Res.*, *82*, 4452-4467, 1977.

Olhoeft, G. R., and D. W. Strangway, Dilectrical properties of the first 100 meters of the Moon, *Earth. Planet. Sci. Letts.*, *24*, 394-404, 1975.

Palluconi, F.D. and H. H. Kieffer, Thermal inertia mapping of Mars from 60S to 60N, *Icarus*, *45*, 415-426, 1981.

Parker, T.J., "Super resolution" of the Mars Pathfinder landing site, using manual techniques, 29th Lunar Planet. Sci. Conf., 1817, 1998.

Presley, M.A. and P. R. Christensen, Thermal conductivity measurements of particulate materials. 2. Results: *J. Geophys. Res., 102, E3*, 6,551-6566, 1997.

Rieder, R., T. Economou, H. Wanke, A. Turkevich, J. Crisp, J. Bruckner, G. Dreibus, H.Y., McSween, The chemical composition of Martian soil and rocks returned by the mobile alpha proton X-ray spectrometer: Preliminary results from the X-ray mode, *Science, 278*, 1743-1748, 1997.

Rover Team, Characterization of the Martian surface deposits by the Mars Pathfinder Rover, Sojourner, *Science, 278*, 1765-1768, 1997.

Smith, P. H., M.G. Tomasko, D. T. Britt, D. G. Crowe, R. Reid, H. U. Keller, N. Thomas, F. Gleim, P. Rueffer, R. Sullivan, R. Greeley, J. M Knudsen, M. B. Madsen, H. P. Gunnlaugsson, S. F. Hviid, W. Goetz, L. A. Soderblom, L. Gaddis, R. Kirk, The imager for Mars Pathfinder experiment, *J. Geophys. Res., 102, E2*, 4003-4025, 1997a.

Smith, P. H., J. F. Bell, III, N. T.Bridges, D. T.Britt, L. Gaddis,, R. Greeley, H. U. Keller, K. E. Herkenhoff, R. Jaumann, J. R. Johnson, R. L. Kirk, M. Lemmon, J. N. Maki, M. C. Malin, S. L. Murchie, J. Oberst, T. J. Parker, R. J. Reid, R. Sablotny, L. A. Soderblom, C. Stoker, R. Sullivan, N. Thomas, M. G. Tomasko, W. Ward, and E. Wegryn, Results from the Mars Pathfinder camera, *Science, 278*, 1758-1765, 1997b.

Terzaghi, Karl, *Theoretical Soil Mechanics*, 509pp., John Wiley and Sons, New York, 1948.

The Rover Team, The Pathfinder Microrover, *J. Geophys. Res., 102, E2*, 3989-4001, 1997.

Kanefsky, B., T.J. Parker, and P.C. Cheeseman, Super-resolution results from Pathfinder IMP, 29th Lunar Planet. Sci. Conf., 1536, 1998.

TABLES

FIGURES

Figure 1. Planview of Pathfinder landing site showing: (a) Sagan Memorial Station (at x=0, y=0), (b) rover traverses (heavy, black lines), and (c) locations of soil mechanics experiments (squares with numbers). Offsets between traverse segments produced by differences between locations predicted with the rover navigation sensors [e.g. *Matijevic,* 1998] and locations determined using the Imager for Mars Pathfinder (IMP or lander camera) images at the end of the day. Coordinate spacings are 2 meters; north is at the top.

Figure 2. Pre-flight photograph of the rover. Rover faces to right and is 32 cm tall. Note: (a) rows of cleats of wheels, (b) strips of nickel, platinum, and aluminum on tread of right center wheel, and (c) rocker-bogie suspension. Solar panel is covered with a dark fabric and undeployed antenna is parallel to edge of panel. Selected features are indicated in Figure 3; dimensions are given in Table 1.

Figure 3. Sketch of the rover, highlighting selected features: (1) rocker-bogie suspension system, (2) wheel used in abrasion experiment, (3) steering motor, (4) wheel motor, (5) tread, (6) front cameras, (7) UHF antenna, solar panel, (8) alpha proton X-ray spectrometer (APXS) and its deployment mechanism, and (9) rear camera.

Figure 4. Rover camera image of wheel track on drift deposit (near 9 in Figure 1). Note: (a) smooth reflective surfaces in track, (b) reflective molds of cleats and spaces between them, (c) rimless depression (upper arrow) formed by compression of drift deposit, (d) slumped surface at right edge of depression. Casper, the bright, irregular object at left edge of frame, may be a coated rock. Casper is about 22 cm wide and 4 cm high. Tracks are 7 cm wide. Image PRODUCT_ID: RVR_EDR-1247909872-N14091-LEFT.

Figure 5. Rover camera image of wheel tracks on drift deposit (northwest of 2 in Figure 1). Note: (a) smooth reflective surfaces in tracks (arrows), (b) reflective molds of cleats and spaces between them (arrow at right), and (c) drift material has been plucked from surface and redeposited as flakes. Tracks are 7 cm wide. Image has been corrected for distortions. Image PRODUCT_ID: RVR_EDR-1247207238-N005524-RIGHT.

Figure 6. Rover image of bright-red drift and exposed surfaces of cloddy deposit in Cabbage Patch (4 in Figure 1). Note: (a) surfaces littered with small fragments, clods, and pebbles, (b) track is only locally reflective, (c) 4 cm diameter pebble, and (d) materials in excavation include granule-size objects and finer ones. Image has been corrected for distortions. Image PRODUCT_ID: RVR_EDR-1247831491-S013158-RIGHT.

Figure 7. Super-resolution color image of rover on Mermaid "dune" (12 in Figure 1). The rover is facing the camera. Piles next to wheels are from excavations during experiment 12. Note that: (a) northeast or facing surfaces of "dune" are darker and grayer than surrounding reddish soil-like deposits, (b) piles from excavations are reddish brown like disturbed soil-like deposits elsewhere, and (c) rocks are chiefly gray. Slope of pile by left rear wheel was estimated to be 32.4° using monoscopic techniques. Image compiled by co-adding end-of day rover IMP image sequences to sharpen surface detail around the rover and reduce noise [*Parker*, 1998; *Kanefsky*, et al., 1998]. Image courtesy of T. J. Parker, Jet Propulsion Laboratory.

Figure 8. IMP image of rover with APXS deployed on Scooby Doo (5 in Figure 1) on Sol 14. Scooby Doo may be an indurated soil-like deposit or a coated rock (see Figure 4). Note that adjacent deposits appear to overlie Scooby Doo. Rover is 32 cm high. Image PRODUCT_ID: IMP_EDR-1247909325-REGULAR-0055360002.

Figure 9. Mosaic of two IMP image of rover showing (1) APXS deployed on surface (sample A-4), (2) excavation in cloddy deposit produced by right rear wheel during soil mechanics experiment (2 in Figure 1), (3) rover track with scattered reflective surfaces and low rims, (4) right center wheel immersed in cloddy deposit after wheel abrasion experiment, (5) excavation in cloddy deposit produced by right front wheel during soil mechanics experiment, and (6) Pop Tart - a probable crust that was displaced by right front wheel during soil mechanics experiment. Rover is 32 cm high. . Slope of pile by right rear wheel was estimated to be 38.3° using IMP images and

stereometric techniques. These two image frames were converted to linear coordinates before combinig them in a mosaic: PRODUCT_ID_IMP_EDR-1247034715-REGULAR-0055290004: IMP_EDR-1247034705-REGULAR-0055290002.

Figure 10. Mosaic of two IMP images of left front wheel above surface during a no-load current measurement on Sol 20 (near 8 in Figure 1). This experiment is called "pop-a-wheelie." These two image frames were converted to linear coordinates before combinig them in a mosaic: PRODUCT_ID: IMP_EDR-1248449645-REGULAR-0054160002 and IMP_EDR- 1248449659-REGULAR-0054160004.

Figure 11. Estimates of the apparent coefficient of friction (tan α) and fraction of the weight of the vehicle on left rear wheel as a function of time during the second rear wheel rotation of experiment 12 (Table 4).

Figure 12. Least squares fit to the paired concurrent values of shear (S) and normal (N) stresses for experiment 3 in cloddy deposit (Table 4).

Figure 13. IMP image of wheel tracks on Mermaid "dune" (see Figure 7; 12 in Figure 1). Note: (a) excavation pile, (b) indentation produced by deployment of APXS for sample A-15, (c) reflective surfaces in tracks, and (d) area where wheel dug into surface. Tracks are 7 cm wide. Image PRODUCT_ID: IMP_EDR-1249596532-REGULAR-0053120002.

Figure 14. Rover image of excavation in lower flank of Mermaid "dune" (12 in Figure 1). Tip of excavation and pile at lower edge is indicated by arrow. Note materials in pile and excavation include granule-size objects and fines. Depth of excavation was about 1 cm; pile is about 8 cm across. Image has been corrected for distortions. Image PRODUCT_ID: RVR_EDR-1249329617-T029066-RIGHT

Figure 15. Three types of depth-time records: (A) layer of weak, porous drift over cloddy material produces two stage record, (B) very thin drift over cloddy deposit with indurated layer or rocks produces complex record with two peaks and flat curve at end, and (C) uniform cloddy deposit produces simple arcuate record.

Figure 16. Rover image of dune-forms hidden from lander camera. These dune-forms could be composed of sand- or granule-sized grains with large thermal inertias, but this is unproved because the rover never drove on or excavated into these dune-forms and then acquired images of the wheel tracks and excavation. Image PRODUCT_IDs for the frames in the mosaic: RVR_EDR-1253411891-N076030-RIGHT, RVR_EDR-1253412760-N076031-RIGHT.

Table 1. Rover characteristics.

Parameter	Value
Deployed Dimensions, cm	
Length	62
Width	47
Height	32
Rover and Payload	
Mass	10.5 kg
Weight on Mars	39.1 N
Nominal Mass per Wheel Pair	
Front	27%
Middle	36%
Rear	37%
Speed	
Nominal	0.4 m/min
Rough Terrain	0.25 m/min
Turning	7 deg. sec
Wheels (six), cm	
Diameter	13
Width	7
Drive Motors (six)	
No-load currents	9-13 mA
Torque factor (above no-load)	3.9-4.4 N-m/mA
Voltage, nominal	15.5 v
Stall torque	3.0-4.5 N-m
Stall current, nominal at 0 deg. C	196 mA

Table 2. Rover camera characteristics

Parameter	Value
General Camera Features	
Charge coupled device array size	768 X 484 pixels
Lens focal length	4 mm
Forward camera separation	12.56 cm
Approximate height above surface	26 cm
Fields of view, degrees	
Forward, cross track	127.5
Forward, along track	94.5
Aft, cross track	94.5
Aft, along track	127.5
Calibrated field. approximate	
Resolutions, mrad, degrees	
Forward, cross track	2.897, 0.166
Forward, along track	3.409, 0.195
Aft, cross track (approx.)	3.409, 0.195
Aft, along track (approx.)	2.897, 0.166
Boresight Angle, degrees	
Forward	-22.5
Aft	-41.4
Wavelength Sensitivity, nm	
Forward	830-890
Aft, approximate red	600-750
Aft, approximate green	500-600
Aft, approximate infrared	700-800

Table 3. Generalized Baseline Soil Mechanics Experiment.

1. Move to experiment site.
2. Acquire rear rover camera image of experiment area.
3. Rotate right rear wheel one turn forward in quarter-turn steps.
4. Acquire rear rover camera image of wheel in excavation.
5. Acquire lander camera stereo-pair image of wheel in excavation.
6. Move forward 20 cm.
7. Acquire rear rover camera image of excavation.
8. Rotate right front wheel one turn forward in quarter-turn steps with 0.0075 turns of the right center wheel backward after each quarter-turn.
9. Align left front and two rear steering motors to push on right front.
10. Acquire right front rover camera image of experiment area.
11. Move forward 8 cm.
12. Acquire lander camera stereo-pair image of wheel in excavation.
13. Acquire left front rover camera image of surface in front of right front wheel.
14. Acquire right front rover camera image of surface in front of right front wheel.
15. Move backward 8 cm.

Table 4. Results of soil mechanics experiments performed by the Pathfinder rover, Sojourner. Values of Φ and c with asterisks used for average cloddy deposit; cloddy deposit of experiment 14 excluded because it is thin.

Exp. No.	Sol	Wheel	No. Turns	Temp °C	No-load (mA)	Y (eq.2) (in-lb/ mA)	Depth (cm)	tan (α) ave.	α (deg.)	Φ_0 (if c=0) (deg.)	Φ fits to S-N (deg.)	c fits to S-N (kPa)	Θ repose angle (deg.)	Material	X (m)	Y (m)
1	3	LF	-0.25		10.3	0.452	0.4	0.850	40.4	37.0	--	--	nd	Cloddy, off ramp	1.5	-1.5
2	4	RR	+1.0	6.0	11.3	0.448	1.6	0.853	40.5	40.1	36.4*	0.27*	38.3	Cloddy, near Yogi	2.8	-2.5
		RF	+1.0	1.8			0.2									
3	13	RR	+1.0	-2.4	11.3	0.455	1.3	0.890	41.4	41.3	40.9*	0.06*	38.3	Cloddy, near Yogi	3.3	-1.3
		RF	+1.0	-2.4			0.2									
4	13	RR	+1.0	0.3	11.3	0.455	3.6	0.836	39.9	39.4	37.3*	0.12*	36.8	Cloddy, Cabbage	3.3	0.0
		RR	+0.5				0.0-3.0	0.900	42.0	39.9	33.6	0.41		Patch		
		RR	+0.5				3.0-3.6	0.809	40.0	38.5	38.3	0.01				
5	15	RR	+0.25		11.3	na	0.0	na				large	nd	Indurated, Scooby Doo	3.1	1.2
6	18	LF	-1.0				1.3								2.6	-1.2
7	18	LF	-1.0				0.4								2.6	0.0
8	21	LR	+1.5	-6.7	12.3	0.460	6.0	0.818	39.3	39.2	38.6*	0.04*	38.3	Cloddy	3.4	-0.7
9	23	RF	-1.0	-0.2	10.3	0.452	0.8	0.495	26.3		26.4	0.53		Drift, near Casper	3.4	1.1
10	27	RR	+1.5	-1.3	11.3	0.454	3.8	0.817	39.2	37.9	35.2*	0.23*	34.0	Cloddy	-2.4	4.4
		RR	+0.35				0.0-0.9	0.686	34.4	36.8	38.6	-0.23		Cloddy		
		RR	+1.15				0.9-3.8	0.879	41.3	40.5	31.4	0.44		Cloddy		
11	27	RR	+1.5	-0.9	11.3	0.453	4.3	0.767	37.5	36.6	33.1	0.22	34.0	Drift / Cloddy	-2.9	4.2
		RR	+0.24				0.0-1.2	0.648	32.9	30.3	27.9	0.18		Drift		
		RR	+1.26				1.2-4.3	0.801	38.7	39.2	40.9*	-0.11*		Cloddy		
12	29	LR	+1.5	-35	12.3	0.497	3.2	0.652	33.1	37.7	33.8*	0.26*	32.4	Mermaid / Cloddy	-5.6	2.6
		LR	+0.33				0.0-1.3	0.697	34.9	34.8	34.7	0.01		Mermaid		
		LR	+1.17				1.3-3.2	0.841	40.1	39.9	37.4	0.15		Cloddy		
		RF	-1.0				0.9								-5.6	3.0
		LR	+1.5	-32	12.3	0.493	1.5	0.723	35.9	35.0	31.7*	0.20*	32.4	Mermaid	-6.2	2.5
13	32	RR	+1.5	7.9	11.3	0.442	1.3	0.809	40.0	38.7	31.6	0.57		Drift/ Cloddy / Rocky	-8.6	0.1
		RR	+0.18				0.0-0.3	0.406	22.1	21.5	15.1	0.43	nd	Drift		
		RR	+0.21				0.3-1.4	0.905	42.2	40.9	35.3*	0.52*		Cloddy		
		RR	+0.41				1.0-1.3	0.867	40.9	40.9	41.1	-0.02		Rocky		
14	74	RR	+1.5	9.0	11.3	0.440	0.5	0.860	40.7	40.9	42.4	-0.20	nd	Cloddy / Rock	-11.5	-3.0
		RR	+0.46				0.0-0.48	0.821	39.4	40.0	42.2	-0.34		Cloddy		
		RR	+1.04				0.48-0.5	0.879	41.3	41.4	45.2	-0.53		Rock		

Table 5. Properties of materials used in tests conducted at the Jet Propulsion Laboratory for the Mars Pathfinder Rover and lunar soil simulants used for the Lunar Roving Vehicle [*Costes, Farmer, and George*, 1972]. Columns labeled wheel, plate, and triaxial are for tests using different methods.

Soil Type	Density kg/m^3	Friction Angle degrees			Cohesion kPa		
		Wheel	Plate	Triaxial	Wheel	Plate	Triaxial
TESTS AT JET PROPULSION LABORATORY							
Loose sand, well-sorted	1342	31.1	33.4	na	0.25	0.07	na
Compacted sand, " "	1507	31.5	34.5	na	0.19	0.07	na
Loose sand, poorly-sorted	1464	33.0	35.0	na	0.24	0.10	na
Compacted sand, " "	1644	35.5	36.9	na	0.13	0.10	na
Loose lunar nominal	1313	34.4	35.0	na	0.29	0.11	na
Compact lunar nominal	1594	37.3	39.3	na	0.17	0.11	na
LUNAR ROVING VEHICLE TESTS							
Loose sand - Yuma	1320	na	28.1	34.6	na	0.83	0.28
Loose lunar nominal	1460	na	31.2	38.4	na	2.14	1.10
Loose lunar nominal	1520	na	34.0	38.5	na	0.97	0.00
Compact lunar nominal	1660	na	35.5	40.0	na	1.03	0.60

Table 6. Grain size distributions of the well-sorted sand, poorly- sorted sand, and lunar nominal soil-like material (crushed basalt) used in the tests of the rover wheel (see Table 5).

Sieve opening mm	well-sorted sand percent retained	well-sorted sand percent finer	poorly-sorted sand percent retained	poorly-sorted sand percent finer	Sieve opening mm	lunar nominal percent retained	lunar nominal percent finer
3.35			0.0	5.5			
					2.83		5.0
2.00			5.5	8.7			
1.70	0.0	0.5	3.2	22.9	1.68	5.0	21.0
1.00	0.5	39.3	14.2	36.6			
0.710	38.8	91.4	13.7	52.1			
0.500	52.1	97.7	15.5	61.4			
0.425	6.3	99.4	9.3	75.1			
0.300	1.7	99.5	13.7	79.8	0.297	16.0	34.0
0.250	0.1		4.7	85.1			
0.180	0.0		5.3	88.2			
					0.149	13.0	50.0
0.125			3.1	89.7			
0.090			1.5	91.1			
0.075			1.4	91.8	0.074	16.0	100.00
0.063			0.7	100.00			

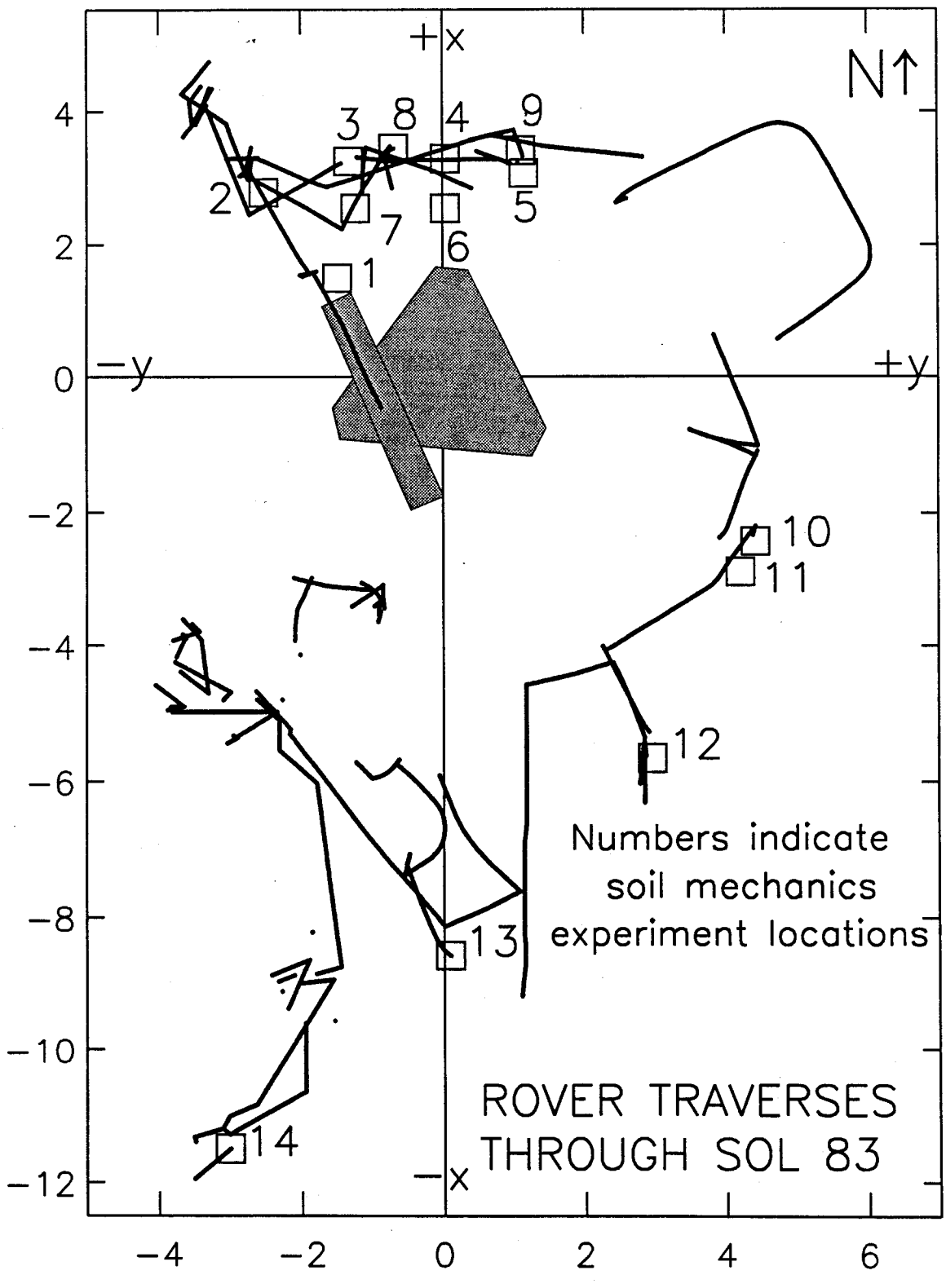
+x
N↑
4
2
0
−2
−4
−6
−8
−10
−12
−y
+y
−x
−4
−2
0
2
4
6
1
2
3
4
5
6
7
8
9
10
11
12
13
14
Numbers indicate
soil mechanics
experiment locations
ROVER TRAVERSES
THROUGH SOL 83

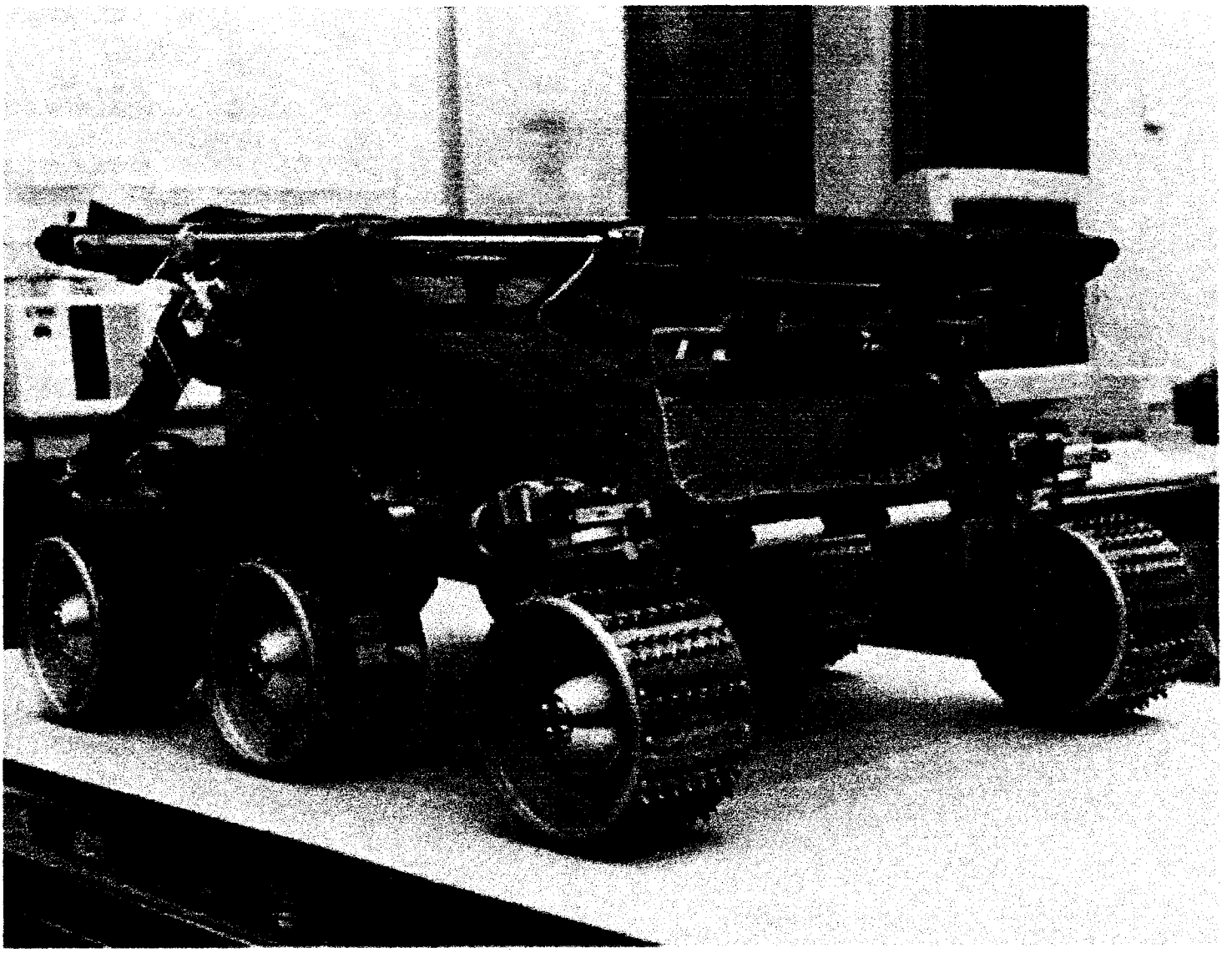

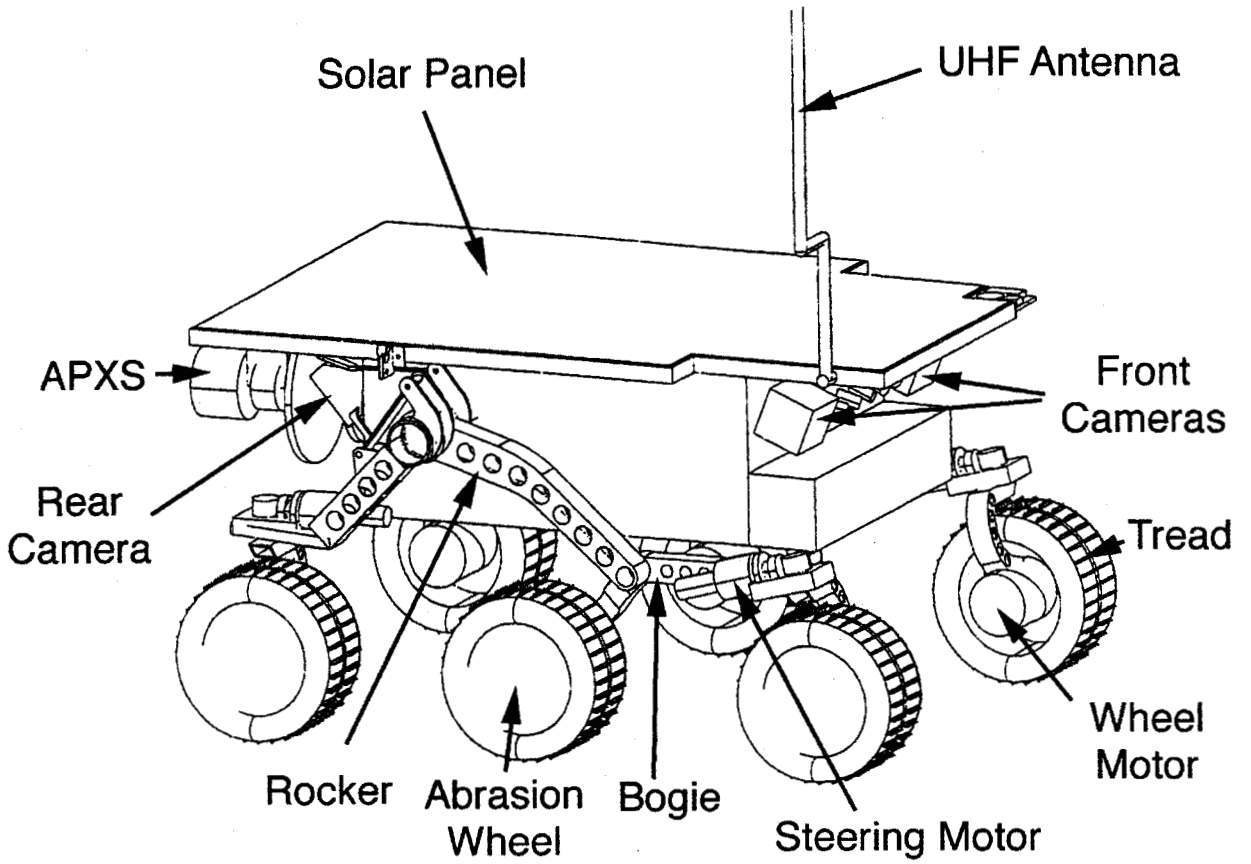
Solar Panel
UHF Antenna
APXS
Front
Cameras
Rear
Camera
Tread
Wheel
Motor
Rocker
Abrasion
Wheel
Bogie
Steering Motor

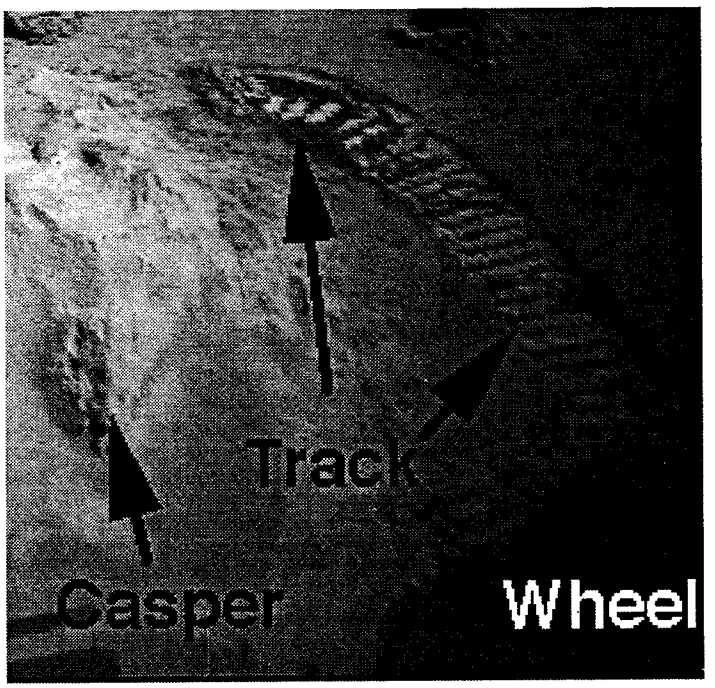
Track
Casper
Wheel

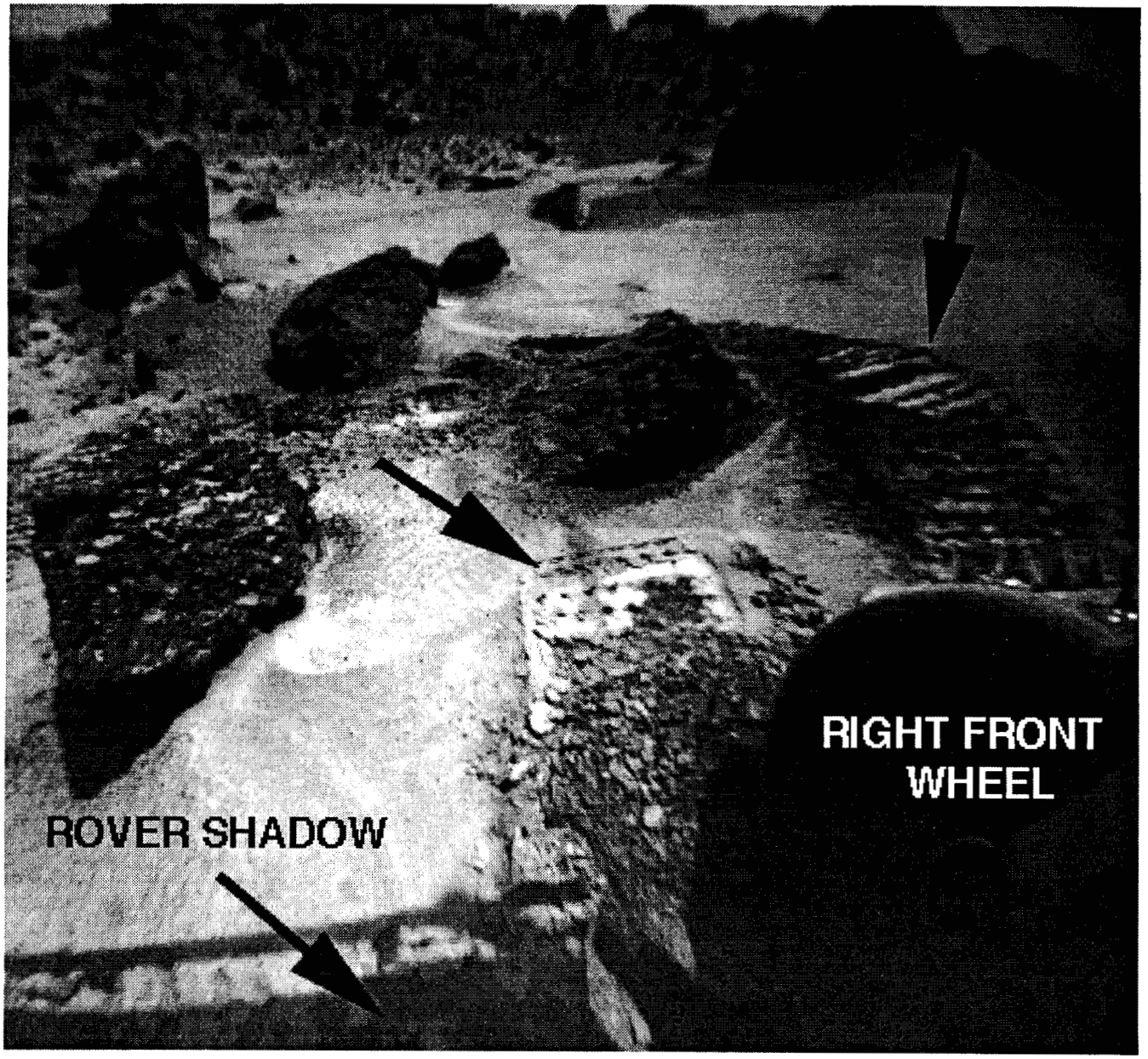
RIGHT FRONT
WHEEL
ROVER SHADOW

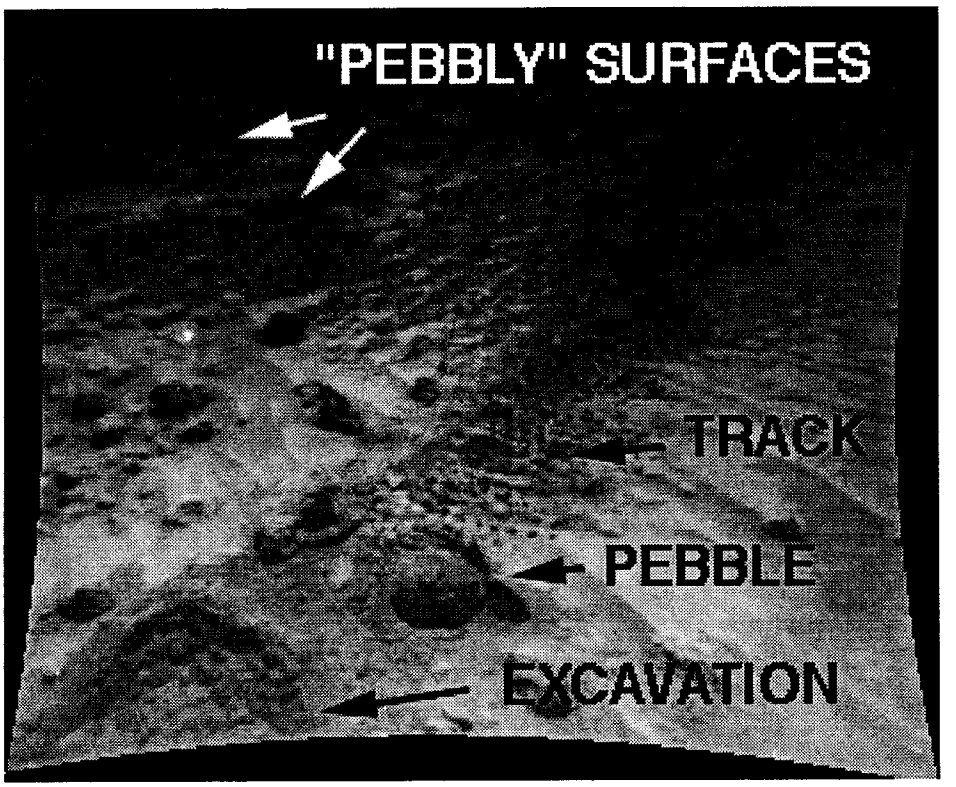
"PEBBLY" SURFACES
TRACK
PEBBLE
EXCAVATION

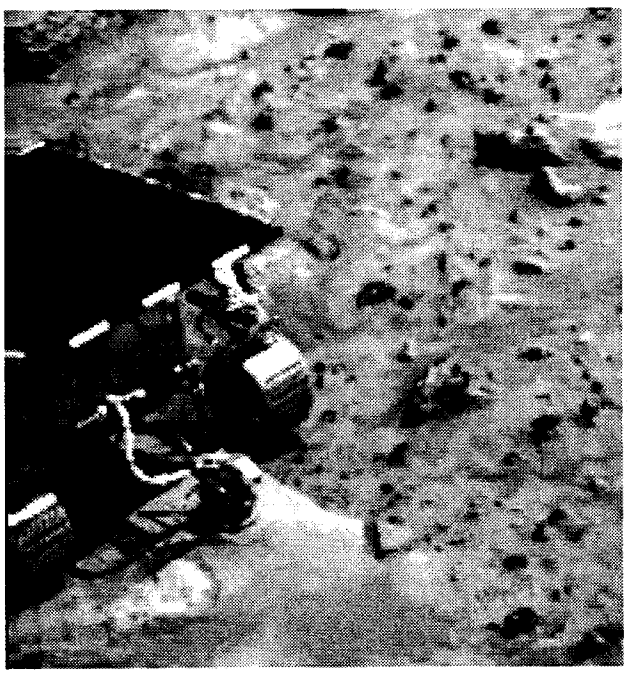

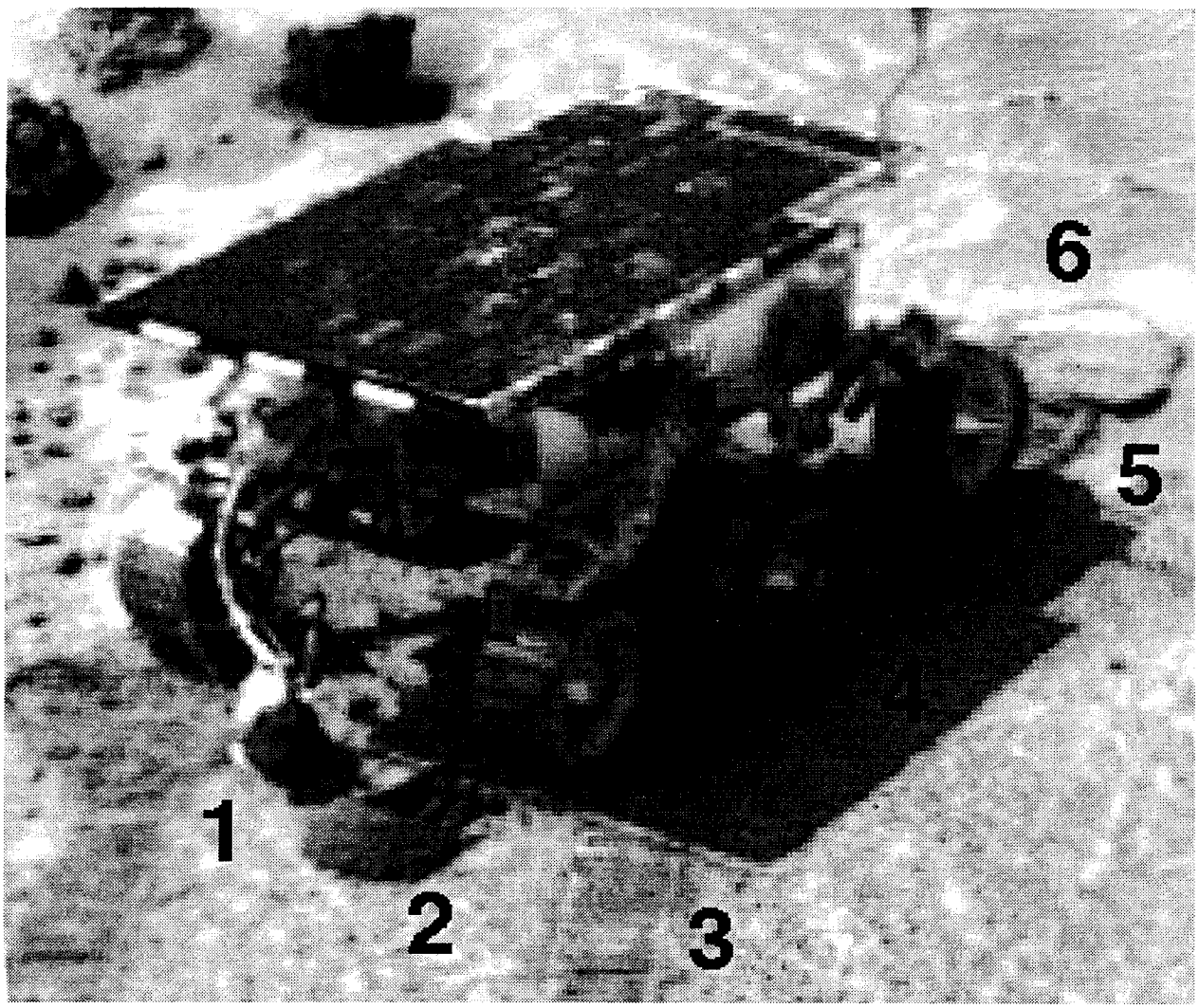
6
5
1
2
3

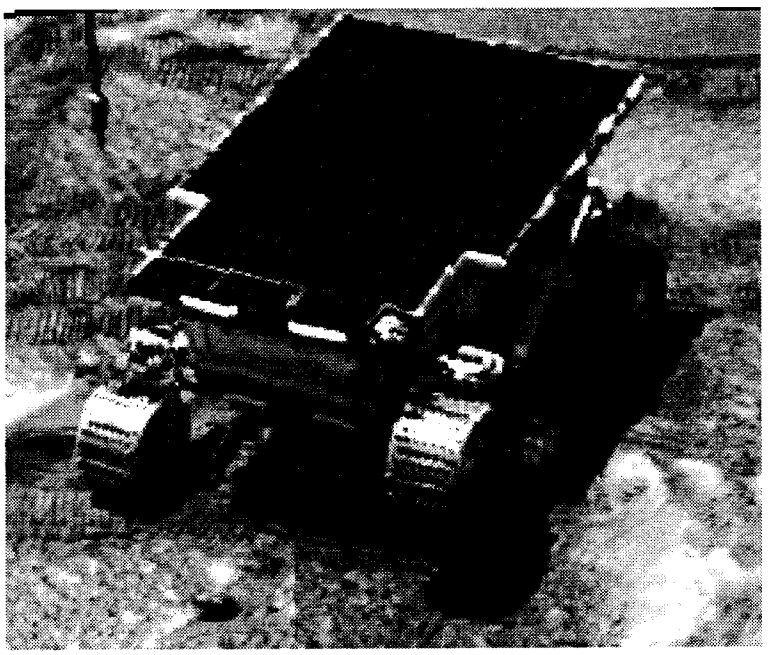

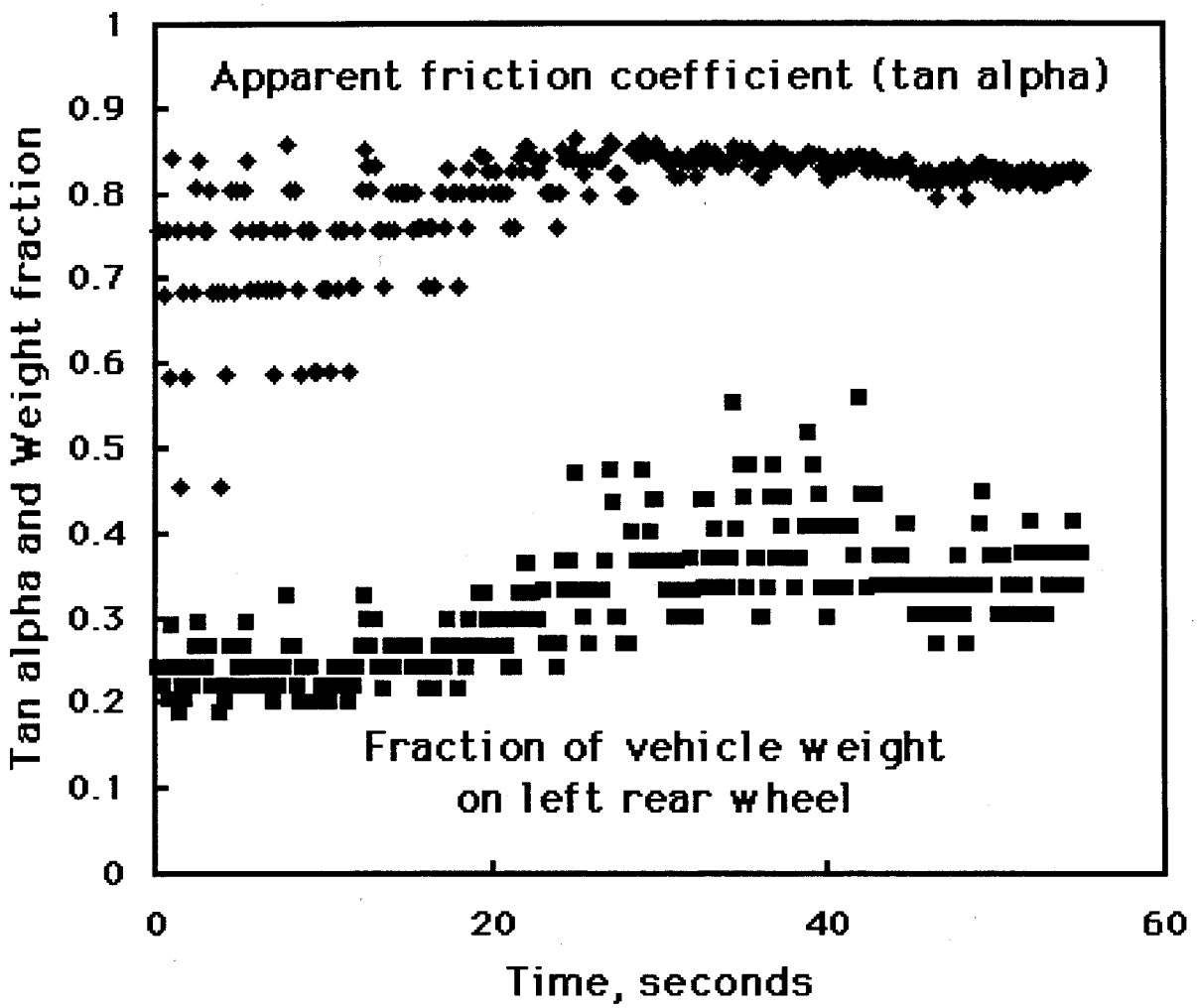
Apparent friction coefficient (tan alpha)
Fraction of vehicle weight
on left rear wheel
Tan alpha and Weight fraction
Time, seconds
1
0.9
0.8
0.7
0.6
0.5
0.4
0.3
0.2
0.1
0
0
20
40
60

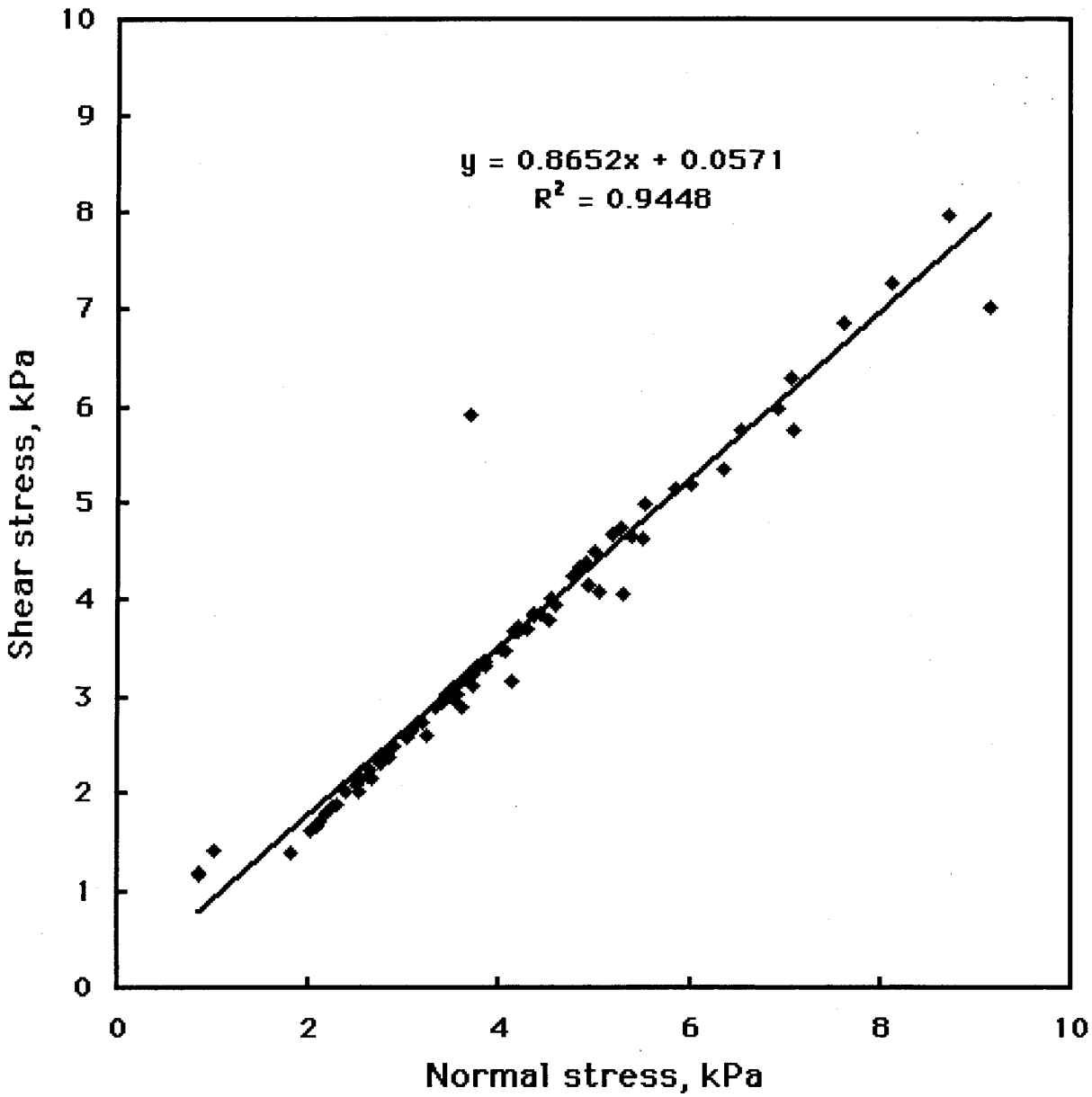
y = 0.8652x + 0.0571
R² = 0.9448
Shear stress, kPa
Normal stress, kPa
0
1
2
3
4
5
6
7
8
9
10
0
2
4
6
8
10

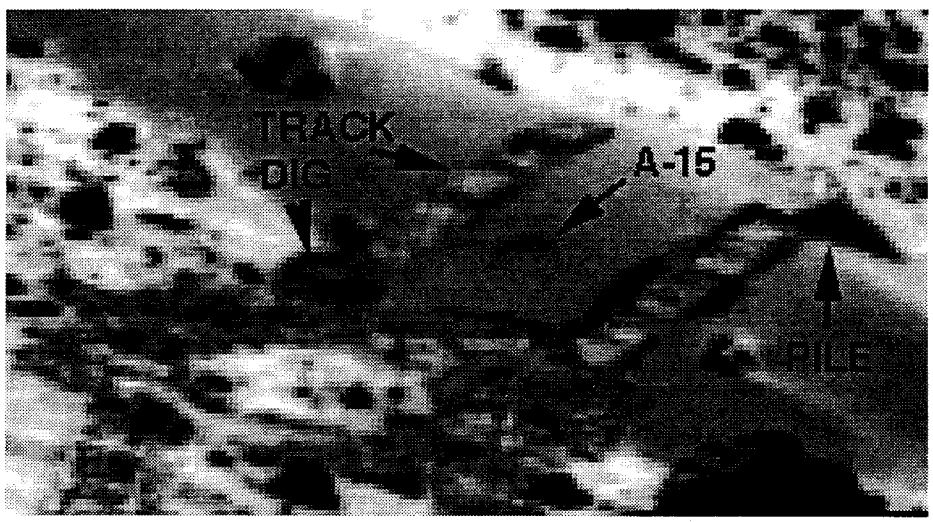
TRACK
DIG
A-15
PILE

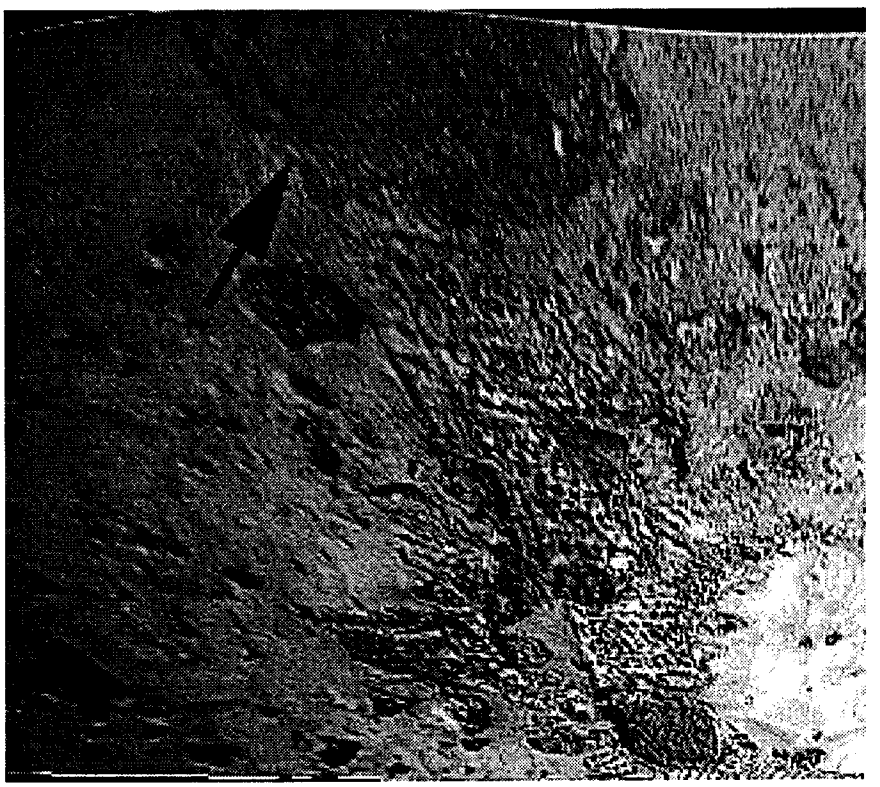

A
Experiment 11
Sol 27
B
Experiment 13
Sol 32
C
Experiment 2
Sol 4
Depth, centimeters
Time, seconds
0
0.5
1
1.5
2
2.5
3
3.5
4
4.5
0
3.8
7.6
11.4
15.2
19
22.8
26.6
30.4
34.2
38
41.8
45.6
49.4
53.2